JACS
JOURNAL OF THE AMERICAN CHEMICAL SOCIETY
Article
pubs.acs.org/JACS

Proton-Conductive Magnetic Metal–Organic Frameworks, $\{NR_3(CH_2COOH)\}[M_a^{II}M_b^{III}(ox)_3]$: Effect of Carboxyl Residue upon Proton Conduction

Hisashi Ōkawa,[†,‡,§,*] Masaaki Sadakiyo,[†,#] Teppei Yamada,[†,∥] Mitsuhiko Maesato,[†] Masaaki Ohba,[‡,§] and Hiroshi Kitagawa[†,§,*]

[†]Division of Chemistry, Graduate School of Science, Kyoto University, Kitashirakawa-Oiwakecho, Sakyo-ku, Kyoto 606-8502, Japan
[‡]Department of Chemistry, Faculty of Science, Kyushu University, Hakozaki 6-10-1, Higashi-ku, Fukuoka 812-8581, Japan
[§]JST-CREST, Gobancho 7, Chiyoda-ku, Tokyo 102-0076, Japan

Supporting Information

ABSTRACT: Proton-conductive magnetic metal–organic frameworks (MOFs), $\{NR_3(CH_2COOH)\}[M_a^{II}M_b^{III}(ox)_3]$ (abbreviated as **R–M_aM_b**: R = ethyl (Et), *n*-butyl (Bu); M_aM_b = MnCr, FeCr, FeFe) have been studied. The following six MOFs were prepared: **Et–MnCr**·$2H_2O$, **Et–FeCr**·$2H_2O$, **Et–FeFe**·$2H_2O$, **Bu–MnCr**, **Bu–FeCr**, and **Bu–FeFe**. The structure of **Bu–MnCr** was determined by X-ray crystallography. Crystal data: trigonal, *R*3*c* (#161), a = 9.3928(13) Å, c = 51.0080(13) Å, Z = 6. The crystal consists of oxalate-bridged bimetallic layers interleaved by $\{NBu_3(CH_2COOH)\}^+$ ions. **Et–MnCr**·$2H_2O$ and **Bu–MnCr** (R–MnCr MOFs) show a ferromagnetic ordering with T_C of 5.5–5.9 K, and **Et–FeCr**·$2H_2O$ and **Bu–FeCr** (R–FeCr MOFs) also show a ferromagnetic ordering with T_C of 11.0–11.5 K. **Et–FeFe**·$2H_2O$ and **Bu–FeFe** (R–FeFe MOFs) belong to the class II of mixed-valence compounds and show the magnetism characteristic of Néel N-type ferrimagnets. The Et-MOFs (**Et–MnCr**·$2H_2O$, **Et–FeCr**·$2H_2O$ and **Et–FeFe**·$2H_2O$) show high proton conduction, whereas the Bu–MOFs (**Bu–MnCr**, **Bu–FeCr**, and **Bu–FeFe**) show moderate proton conduction. Together with water adsorption isotherm studies, the significance of the carboxyl residues as proton carriers is revealed. The R–MnCr MOFs and the R–FeCr MOFs are rare examples of coexistent ferromagnetism and proton conduction, and the R–FeFe MOFs are the first examples of coexistent Néel N-type ferrimagnetism and proton conduction.

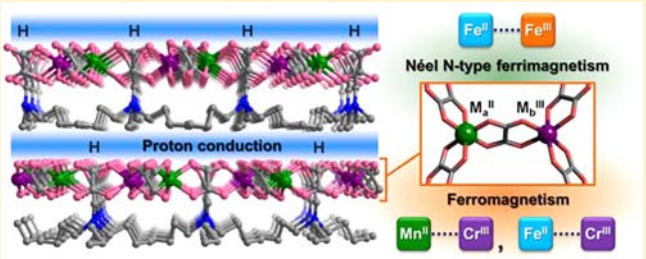

INTRODUCTION

The development of proton-conductive materials is important because of their potential in solid-state electrochemical devices such as batteries and fuel cells.[1−4] The proton-conductive properties of inorganic metal oxides such as $SrZrO_3$ and inorganic acid salts such as $CsHSO_4$ have been explored.[4a] Polymer electrolyte membranes such as Nafion are a class of synthetic proton-conductive materials that have been extensively studied.[5−10] Recent work on proton-conductive materials has been based on metal–organic frameworks (MOFs),[11−20] where proton pathways are potentially designable in the frameworks.[14] Among them, the MOFs of the formula $(A)[M_a^{II}M_b^{III}(ox)_3]$, first developed as molecular-based magnets,[21,22] have a high prospect of producing functional materials by introducing functionality into the cationic component. To date, paramagnetic,[23] photoactive,[24] conductive,[25] or chiral cationic ions[26] have been used with the intention of producing functional magnetic materials. Our strategy for producing proton-conductive materials based on $(A)[M_a^{II}M_b^{III}(ox)_3]$ is to introduce acidic or hydrophilic residues into the cationic component so as to construct proton-conductive pathways between the bimetallic layers.[19,20] Such MOFs must be valuable for studying the interplay of proton conduction and magnetism, that is, spin-protonics.[19,20] We earlier reported the MOFs of tri(3-hydroxypropyl)ammonium ion, $\{NH(prol)_3\}[MCr(ox)_3]\cdot 2H_2O$,[19] in which the hydroxyl residues of the cationic components function as proton mediators to allow appreciably high proton conduction coexistent with ferromagnetism.

In this article, we report proton-conductive magnetic MOFs of trialkyl(carboxymethyl)ammonium ions, $\{NR_3(CH_2COOH)\}[M_a^{II}M_b^{III}(ox)_3]$ (abbreviated as **R–M_aM_b**: R = Et (ethyl) or Bu (*n*-butyl); M_aM_b = MnCr, FeCr or FeFe). The following MOFs were prepared: **Et–MnCr**·$2H_2O$, **Et–FeCr**·$2H_2O$, **Et–FeFe**·$2H_2O$, **Bu–MnCr**, **Bu–FeCr**, and **Bu–FeFe**. We expected that the carboxyl residues of the cationic components would function as proton carriers to bring about efficient proton conduction. The magnetic properties of the MOFs were studied with respect to the M_aM_b combination, and the proton-conductive properties were examined in view of the cationic ions. It is notable that the mixed-valence $Fe^{II}Fe^{III}$ MOFs, **Er–FeFe**·$2H_2O$, and **Bu–**

Received: October 9, 2012
Published: January 9, 2013

dx.doi.org/10.1021/ja309968u | J. Am. Chem. Soc. 2013, 135, 2256−2262

FeFe are the first examples of coexistent rare Néel N-type ferrimagnetism and proton conduction. Through this work, we also search for a clue to multifunctional materials with cooperative magnetism and proton conduction.

EXPERIMENTAL SECTION

The literature method[27] was used for the preparation of $(NH_4)_3[Cr(ox)_3]\cdot 3H_2O$ and $(NH_4)_3[Fe(ox)_3]\cdot 3H_2O$. Other chemicals were of reagent grade and were used as purchased.

Preparation of {NR$_3$(etac)}Br. *{NEt$_3$(CH$_2$COOH)}Br.* A mixture of ethyl bromoacetate (3.5 g), triethylamine (2.1 g), and ethanol (5 cm^3) was stirred under reflux for 3 h. On evaporating the solvent, $\{NEt_3(CH_2COOEt)\}Br$ was obtained as an oily substance. It was dissolved in water (70 cm^3) and a few drops of conc. HBr were added to the solution, and the mixture was stirred at ca. 60 °C for 12 h. The reaction mixture was evaporated to dryness and the resulting semisolid was crystallized from ethanol as colorless prisms. The yield was 3.4 g. Elemental analyses (%) Calcd. for $C_8H_{18}NO_2Br$: C, 40.01; H, 7.56; N, 5.83%. Found: C, 39.76; H, 7.71; N, 5.74%. FTIR/cm^{-1}: 1742.

{NBu$_3$(CH$_2$COOH)}Br. This was obtained as an oily substance in a similar way to that described above, except for the use of tri(*n*-butyl)amine (3.7 g) instead of triethylamine. The yield of the crude product was 4.9 g. FTIR/cm^{-1}: ∼1740. It was used for preparing MOFs without further purification.

Preparation of R−M$_a$M$_b$ MOFs. ***Et−MnCr·2H$_2$O.*** $(NH_4)_3[Cr(ox)_3]\cdot 3H_2O$ (210 mg) and $MnCl_2\cdot 4H_2O$ (100 mg) were stirred in methanol (15 cm^3) for a while and the mixture was filtered to separate any insoluble materials. A solution of $\{NEt_3(CH_2COOH)\}Br$ (120 mg) in methanol (10 cm^3) was added and the mixture was stirred at ambient temperature. The resulting purple crystals were separated by filtration, washed with methanol, and dried over silica gel in a vacuum desiccator. Yield: 170 mg. Elemental analyses (%) Calcd. for $C_{14}H_{22}NO_{16}CrMn$: C, 29.64; H, 3.91; N, 2.47; Cr, 10.93; Mn, 9.68%. Found: C, 29.53; H, 3.65; N, 2.57; Cr, 10.53; Mn, 10.02%. FTIR/cm^{-1}: 1635. Visible bands on powder (λ/nm): 560, ∼405, 260. μ_{eff}/MnCr: 7.14 μ_B at 300 K.

Et−FeCr·2H$_2$O. This was prepared by reacting $(NH_4)_3[Cr(ox)_3]\cdot 3H_2O$ (210 mg), $FeCl_2\cdot 4H_2O$ (100 mg), and $\{NEt_3(CH_2COOH)\}Br$ (120 mg) in methanol (20 cm^3). The resulting brown microcrystals were filtered, washed with methanol, and dried over silica gel in vacuo. Yield: 185 mg. Elemental analyses (%) Calcd. for $C_{14}H_{22}NO_{16}CrFe$: C, 29.60; H, 3.90; N, 2.47; Cr, 9.15; Fe, 9.83%. Found: C, 29.54; H, 3.79; N, 2.49; Cr, 9.51; Fe, 10.12%. FTIR/cm^{-1}: 1635. Visible bands on powder (λ/nm): ∼560, ∼400, and ∼270. μ_{eff}/FeCr: 7.20 μ_B at 300 K.

Et−FeFe·2H$_2$O. A mixture of $(NH_4)_3[Fe(ox)_3]\cdot 3H_2O$ (215 mg) and $FeCl_2\cdot 4H_2O$ (100 mg) in methanol (20 cm^3) was stirred for 15 min and filtered to separate any insoluble material. To the filtrate, a solution of $\{NEt_3(CH_2COOH)\}Br$ (120 mg) in methanol (10 cm^3) was added dropwise and the mixture was stirred at room temperature for 30 min. The deep-green microcrystals thus precipitated were separated by filtration, washed with methanol, and dried over silica gel in a vacuum desiccator. Yield: 140 mg. Elemental analyses (%) Calcd. for $C_{14}H_{22}NO_{16}Fe_2$: C, 29.39; H, 3.88; N, 2.45; Fe, 19.53%. Found: C, 29.54; H, 3.89; N, 2.48; Fe, 19.31%. Visible band on powder (λ/nm): ∼660. FTIR/cm^{-1}: 1635. μ_{eff}/$Fe^{II}Fe^{III}$: 7.10 μ_B at 300 K.

Bu−MnCr. This was obtained as purple microcrystals by a method similar to that for **Et−MnCr**·2H$_2$O except for the use of $\{NBu_3(CH_2COOH)\}Br$ (175 mg) instead of $\{NEt_3(CH_2-COOH)\}Br$. Yield: 255 mg. Elemental analyses (%) Calcd. for $C_{20}H_{30}NO_{14}CrMn$: C, 39.03; H, 4.91; N, 2.28; Cr, 8.45; Mn, 8.93%. Found: C, 38.74; H, 5.05; N, 2.50; Cr, 8.27; Mn, 9.26%. FTIR/cm^{-1}: 1635. Visible bands on powder (λ/nm): 560, 405, and ∼270. μ_{eff}/MnCr: 7.22 μ_B at 300 K.

Bu−FeCr. This was obtained as brown microcrystals by a method similar to that for **Et−FeCr**·2H$_2$O using $\{NBu_3(CH_2COOH)\}Br$ (175 mg) instead of $\{NEt_3(CH_2-COOH)\}Br$. Yield: 270 mg. Elemental analyses (%) Calcd. for $C_{20}H_{30}NO_{14}CrFe$: C, 38.98; H, 4.91; N, 2.27; Cr, 8.44; Fe, 9.06%. Found: C, 38.73; H, 4.99; N, 2.49; Cr, 8.07; Fe, 9.29%. FTIR/cm^{-1}: 1634. Visible bands on powder (λ/nm): ∼570$_{br}$, ∼405, and ∼260. μ_{eff}/FeCr: 7.33 μ_B at 300 K.

Bu−FeFe. This was obtained as deep-green microcrystals in a way similar to that for **Et−FeFe**·2H$_2$O using $\{NBu_3(CH_2-COOH)\}Br$ (170 mg) instead of $\{NEt_3(CH_2COOH)\}Br$. Yield: 170 mg. Elemental analyses (%) Calcd. for $C_{20}H_{30}NO_{14}Fe_2$: C, 38.74; H, 4.88; N, 2.26; Fe, 18.01%. Found: C, 38.53; H, 4.97; N, 2.23; Fe, 18.32%. Visible bands on powder (λ/nm): ∼665. FTIR/cm^{-1}: 1633. μ_{eff}/$Fe^{II}Fe^{III}$: 7.52 μ_B at 300 K.

Physical Measurements. X-ray powder diffraction (XRPD) measurements were carried out using Bruker D8 ADVANCE (λ = 1.54059 Å; CuKα). Electronic spectra were measured using a powdered sample with CaF_2 using a JASCO V-570 spectrophotometer. Infrared spectra were recorded on a JASCO FTIR-4200 Fourier transform infrared spectrophotometer equipped with ATR. Magnetic measurements were made using a Quantum Design MPMS-XL5R SQUID susceptometer. Diamagnetism correction of constituting atoms was made using Pascal's constants.[28] Measurements of field-cooled magnetization and zero-field-cooled magnetization were performed under an applied field of 5 Oe on the same susceptometer. Thermogravimetric analyses (TGA) were carried out using Bruker TG-DTA 2000SA with heating rate of 5 °C/min under N_2 flow (100 mL/min) condition. Proton conductivities were measured using the impedance method on sample pellets (∼0.8 mm thickness × 2.5 mm ϕ) prepared under a pressure of ∼1.2 GPa. The impedance measurements were carried out at 298 K by a conventional quasi-four-probe method using gold paste and gold wires (50 μm ϕ) with a Solartron 1260 Impedance/Gain−Phase Analyzer and 1296 Dielectric Interface in the frequency range 1 Hz−1 MHz. Relative humidity was controlled using an Espec Corp. SH-221 incubator.[29] Water adsorption isotherms were measured at 298 K with an automatic vapor adsorption apparatus, BELSORP-max (BEL JAPAN). Samples were thoroughly dehydrated prior to the measurement by heating at 373 K for 16 h under vacuum.

Crystal Structure Determination. Purple crystals of **Bu−MnCr** were grown by slow crystallization from a dilute methanol solution of $(NH_4)_3[Cr(ox)_3]\cdot 3H_2O$, $MnCl_2\cdot 4H_2O$ and $\{NBu_3(CH_2COOH)\}Br$ (1:1:1). A single crystal of approximate dimensions of 0.24 × 0.29 × 0.03 mm was used for collecting X-ray diffraction data at 23 °C on a Rigaku AFC-7R diffractometer with graphite-monochromated Mo Kα radiation (λ = 0.71069 Å). The structure was solved by the direct method and expanded using Fourier techniques. All calculations were performed using the *Crystal Structure* crystallographic software package.[30] Full-matrix least-squares

dx.doi.org/10.1021/ja309968u | J. Am. Chem. Soc. 2013, 135, 2256−2262

refinements were carried out using *SHELXL-97*[31] with anisotropic thermal parameters for non-hydrogen atoms.

Crystal data: purple crystals, $C_{20}CrH_{30}MnNO_{14}$, molecular weight = 615.39, trigonal, space group $R3c$ (#161), $Z = 6$, $a = b = 9.3928(13)$ Å, $c = 51.0080(13)$ Å, $V = 3897.3(8)$ Å^3, $D_{calcd} = 1.573$ g cm^{-3}, μ(Mo Kα) = 9.734 cm^{-1}, $R_1 = 0.0519$ ($|I| > 2.0\sigma(I)$), $R = 0.0551$ (all reflections) and $wR_2 = 0.1344$ (all reflections). The symmetry operations: (1): $-Y + 1, X - Y, Z$; (2): $-X + Y + 1, -X + 1, Z$; (3): $-Y + 1, X - Y + 1, Z$; (4): $-X + Y, -X + 1, Z$.

RESULTS AND DISCUSSION

General Characterization. The (A)[$M^{II}Cr^{III}(ox)_3$] MOFs are generally obtained by the reaction of $K_3[Cr(ox)_3]$, an M(II) salt and an A^+ salt in water. However, this method cannot be applied to the MOFs of hydrophilic cationic ions because of the instability of their networks in water. To overcome the problem, we have employed a synthetic procedure that uses $(NH_4)_3[Cr(ox)_3]$ instead of $K_3[Cr(ox)_3]$ in methanol.[19] Using this procedure, the Et−MCr MOFs (**Et−MnCr**·2H_2O and **Et−FeCr**·2H_2O) and the Bu−MCr MOFs (**Bu−MnCr** and **Bu−FeCr**) were obtained in this work. Further, the R−FeFe MOFs (**Et−FeFe**·2H_2O and **Bu−FeFe**) in the $Fe^{II}Fe^{III}$ mixed-valence state were prepared by the use of $(NH_4)_3[Fe(ox)_3]$ in methanol. The Et−MOFs (**Et−MnCr**·2H_2O, **Et−FeCr**·2H_2O, and **Et−FeFe**·2H_2O) are sensitive to moisture and decompose on prolonged standing in open air. The Bu−MOFs (**Bu−MnCr**, **Bu−FeCr**, and **Bu−FeFe**) are stable in open air but readily decompose in water. The results of TGA measurements show that anhydrate states of Et−MOFs are formed by dehydration (approximately 2 water molecules) below 60 °C (Figure S1 of the Supporting Information). Bu−MOFs do not indicate apparent weight loss below 100 °C. The thermal stability of the frameworks were roughly estimated as 200 (for **R−FeFe**), 250 (for **R−FeCr**), and 300 °C (for **R−MnCr**).

The powder reflectance spectra of the R−MnCr MOFs and the R−FeCr MOFs have three absorption bands at 560−570, 400−410, and 260−270 nm attributable to the d−d transition bands of the {$Cr^{III}(ox)_3$} chromophore. The d−d bands of the {$Mn^{II}(ox)_3$} and the {$Fe^{II}(ox)_3$} components are not resolved. The electronic spectra of **Et−FeFe**·2H_2O and **Bu−FeFe** are characterized by an intense band near 650 nm (Figure 1). This can be attributed to the Fe^{II}/Fe^{III} intervalence transition band.[32−36] Together with powder X-ray diffraction studies indicating the valence localization of the iron centers (next section), **Et−FeFe**·2H_2O and **Bu−FeFe** belong to class II of mixed-valence compounds in the classification by Robin and Day.[37]

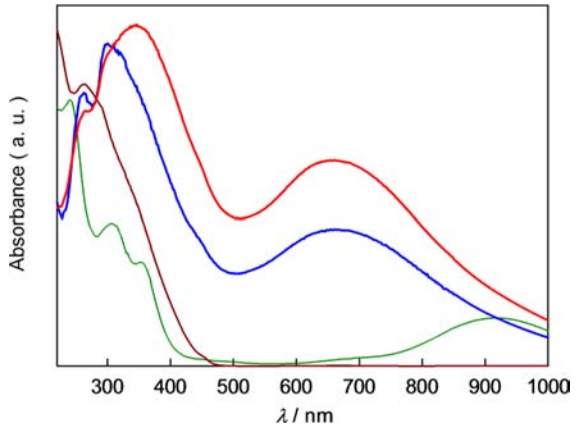

Figure 1. Electronic reflectance spectra of (blue) **Et−FeFe**·2H_2O and (red) **Bu−FeFe**. Spectra of (brown) $(NH_4)_3[Fe(ox)_3]\cdot 3H_2O$ and (green) $FeCl_2\cdot 4H_2O$ are given for comparison.

Structure. The X-ray crystallographic result for **Bu−MnCr** has been briefly reported.[20] The crystal consists of oxalate-extended bimetallic layers and {$NBu_3(CH_2COOH)$}$^+$ ions residing between the layers (Figure 2). The interlayer separation is 8.516 Å. The structural features resemble those of analogous {A}[$M^{II}M'^{III}(ox)_3$] compounds.[19,22−26] A projection of one bimetallic layer along the *ab* plane is shown in Figure 3. Selected bond distances and bond angles are summarized in Table S1 of the Supporting Information. The two metal ions are clearly distinguished by the short Cr−O bonds (av. 1.975 Å) and the long Mn−O bonds (av. 2.189 Å). The {$NBu_3(CH_2COOH)$}$^+$ ions are perpendicularly aligned to the bimetallic layer, with the NBu_3 residues in the interlayer space and the carboxyl residues in each honeycomb cavity. The carboxyl terminal is nearly exposed to the interlayer space. There is a rotational disorder about the $R_3N^+-CH_2-COOH$ linkage. A disorder also exists in the *n*-butyl groups.

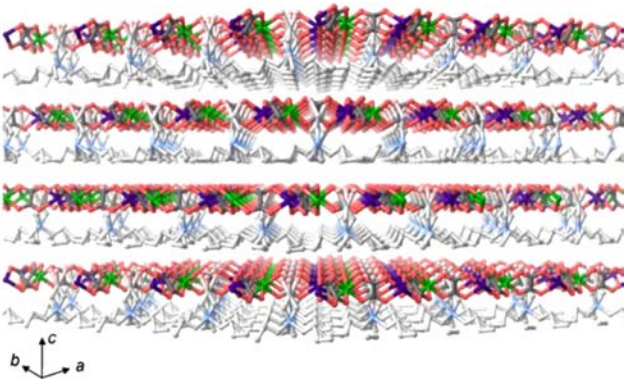

Figure 2. Crystal structure of **Bu−MnCr** (green, Cr; purple, Mn; pink, O; blue, N; gray, C).

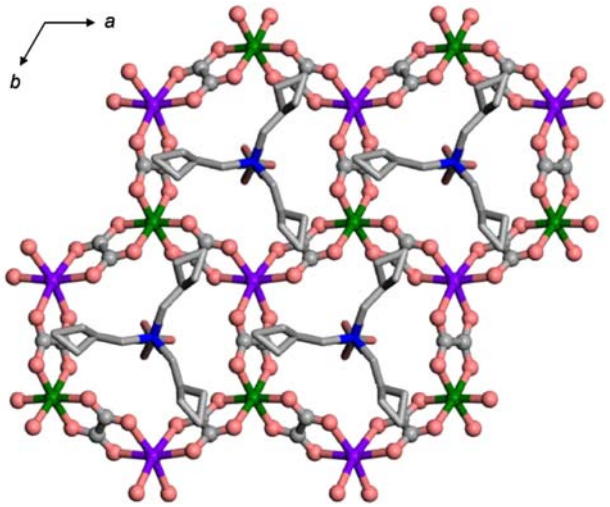

Figure 3. Projection of a metal−oxalate layer and {$NBu_3(CH_2COOH)$}$^+$ ions of **Bu−MnCr** along the *ab* plane (green, Cr; purple, Mn; pink, O; blue, N; gray, C).

dx.doi.org/10.1021/ja309968u | *J. Am. Chem. Soc.* 2013, 135, 2256−2262

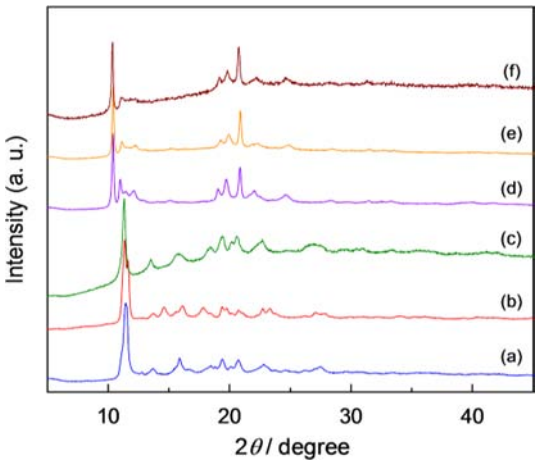

Figure 4. XRPD patterns of (a) **Et−MnCr**·2H_2O, (b) **Et−FeCr**·2H_2O, (c) **Et−FeFe**·2H_2O, (d) **Bu−MnCr**, (e) **Bu−FeCr**, and (f) **Bu−FeFe**.

Powder X-ray diffraction (XRPD) spectra are given in Figure 4. Obviously, **Bu−FeCr** and **Bu−FeFe** are isomorphous with **Bu−MnCr**, to judge from the marked resemblance in the XRPD patterns. The interlayer separation of 8.49 Å is estimated for both **Bu−FeCr** and **Bu−FeFe** based on the highest peak at 2θ ∼10° in the XRPD spectra. The Et−MOFs are also isomorphous. Their interlayer separations are estimated to be 7.73−7.84 Å. The XRPD spectral results indicate that the Fe^{II} and Fe^{III} centers of **Et−FeFe**·2H_2O and **Bu−FeFe** are distinctly localized.

Magnetic Properties. The temperature variations of the magnetic susceptibilities and the magnetic moments of the R−MnCr MOFs and the R−FeCr MOFs are given in Figure 5. The magnetic moments of **Et−MnCr**·2H_2O and **Bu−MnCr** at room temperature are 7.14 and 7.22 μ_B, respectively. The moments increase as the temperature is lowered, very gradually to 10 K and abruptly below 10 K, to a large maximum value near 5 K. The magnetic moments of **Et−FeCr**·2H_2O and **Bu−FeCr** at room temperature are 7.20 and 7.33 μ_B respectively, and the moments increase as the temperature is lowered to a large maximum value near 9 K. The magnetic properties of the R−MnCr MOFs and the R−FeCr MOFs are compared with those of analogous (A)[$MnCr(ox)_3$] and (A)[$FeCr(ox)_3$], respectively.[21−24] The ferromagnetic ordering in the MOFs is proved by weak-field magnetization and ac magnetization studies (Figures S2−S5 of the Supporting Information). The T_C was determined to be 5.9 K for **Et−MnCr**·2H_2O, 5.6 K for **Bu−MnCr**, 11.0 K for **Et−FeCr**·2H_2O, and 11.5 K for **Bu−FeCr**. The T_C values of the R−MnCr MOFs fall in the range of 5.0−6.0 K reported for the analogous (A)[$MnCr(ox)_3$][21−24] and the T_C values of the R−FeCr MOFs fall in the range of 9.5−13.0 K reported for the analogous (A)[$FeCr(ox)_3$].[21,23,24b]

The magnetic moments of **Et−FeFe**·2H_2O and **Bu−FeFe** at room temperature are 7.10 and 7.52 μ_B, respectively. The moments decrease as the temperature is lowered to a minimum value around 47 K and then increase to a maximum value at ∼40 K (Figure 6 and Figure S6 of the Supporting Information). Below 40 K, the magnetic moment decreases rapidly to zero μ_B at 31 K. Weak-field magnetization results of **Et−FeFe**·2H_2O and **Bu−FeFe** are given in Figure 7 and Figure S7 of the Supporting Information, respectively. With lowering temperature, the field-cooled magnetization (FCM) of **Et−FeFe**·2H_2O increases to a small positive value at ∼39 K and then

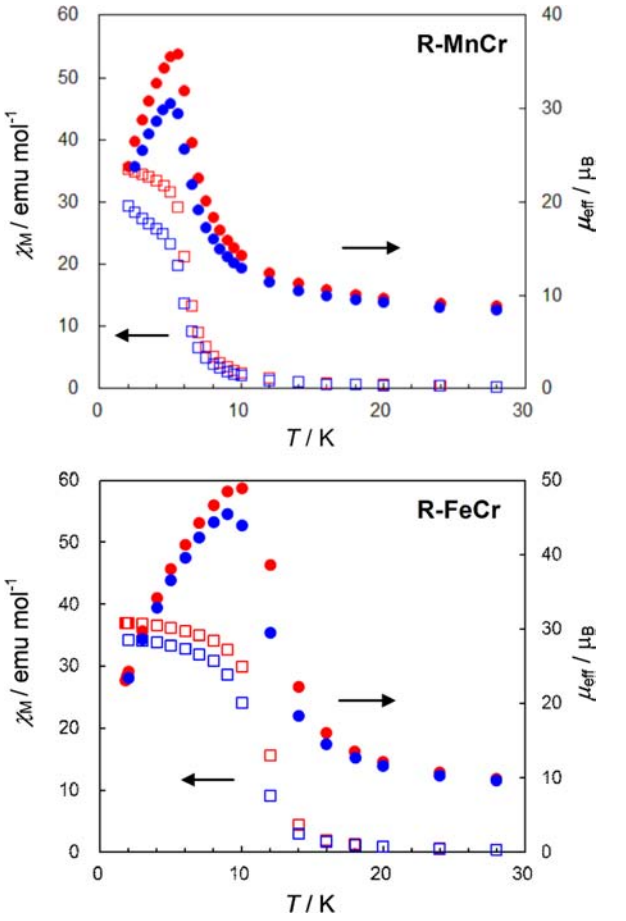

Figure 5. Top, temperature variations of χ_M and μ_{eff} for (blue) **Et−MnCr** and (red) **Bu−MnCr**; bottom, temperature variations of χ_M and μ_{eff} for (blue) **Et−FeCr** and (red) **Bu−FeCr**.

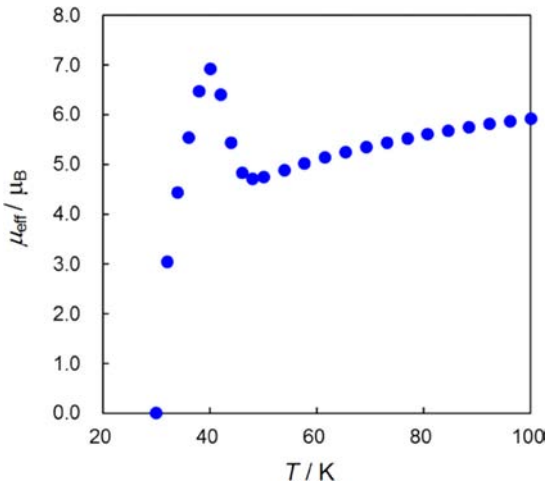

Figure 6. Temperature variation of magnetic moment of **Et−FeFe**·2H_2O.

decreases to a large negative value at 2 K, through the compensation temperature of ∼33 K. When the applied magnetic field is switched off at 2 K, remnant magnetization (RM) of essentially the same negative value as the FCM is observed and the RM follows the FCM curve on warming. The zero-field-cooled magnetization (ZFCM) curve, however, maintains a positive value below 31 K. A similar magnetization

dx.doi.org/10.1021/ja309968u | J. Am. Chem. Soc. 2013, 135, 2256−2262

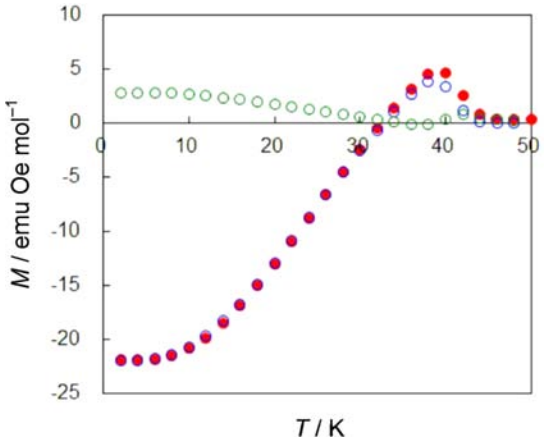

Figure 7. Field-cooled (red) magnetization under 5 Oe, (blue) remnant magnetization, and (green) zero-field-cooled magnetization of **Et−FeFe**·2H_2O.

feature has been recognized for (A)[$Fe^{II}Fe^{III}(ox)_3$] with alkyl-substituted ammonium ions[38,39] and is explained in terms of Néel N-type ferrimagnetism.[39,40] The negative magnetization at low temperatures arises when the Fe^{II} sublattice orders faster than the Fe^{III} sublattice with lowering temperature. Néel N-type ferrimagnetism is versatile in metal oxides[40−44] but very rare in molecular systems[45,46] except for (A)[$Fe^{II}Fe^{III}(ox)_3$] and the R−FeFe MOFs.

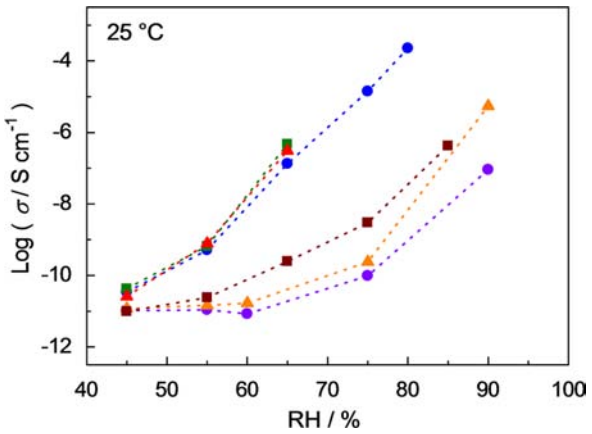

Figure 8. Proton conductivity vs RH profiles at 25 °C of (blue) **Et−MnCr**·2H_2O, (red) **Et−FeCr**·2H_2O, (green) **Et−FeFe**·2H_2O, (purple) **Bu−MnCr**, (orange) **Bu−FeCr**, and (brown) **Bu−FeFe**.

Proton Conduction. Proton conductivities were determined using alternating-current impedance measurements on pellet samples. The log (σ/S cm^{-1}) versus RH (relative humidity) profiles are given in Figure 8. The profiles of **Et−FeCr**·2H_2O and **Et−FeFe**·2H_2O are only shown up to 65% RH because they decomposed near 70% RH. It is noticed that the Et−MOFs have comparable log (σ/S cm^{-1}) versus RH profiles and the Bu−MOFs also have comparable profiles. Thus, the conduction of the R−MOFs is governed by the cationic ions irrespective of the magnetic nature varying with the $M_a^{II}M_b^{III}$ combination. The class II Fe^{II}/Fe^{III} mixed-valence state in the **Et−FeFe**·2H_2O or **Bu−FeFe** is not concerned with the electrical conduction because of their low DC conductivity (less than 10^{-11} Scm^{-1}). The Et−MOFs and Bu−MOFs have similar conductivities at 45% RH ($3 \times 10^{-11} \sim 1 \times 10^{-11}$ S cm^{-1}), but the conductivities of the Et−MOFs increase sharply with RH to $\sim 1 \times 10^{-7}$ S cm^{-1} at 65% RH, whereas the conductivities of the Bu−MOFs increase less sharply to $\sim 1 \times 10^{-7}$ S cm^{-1} near 85% RH. It must be noted that {NBu_4}[$MnCr(ox)_3$] as the reference has a low conductivity of 1.2×10^{-12} S cm^{-1} at 45% RH and the conductivity increases sluggishly with RH to 1.1×10^{-9} S cm^{-1} at 95% RH.[19] Thus, we may conclude that the proton conduction associated with the {$NR_3(CH_2COOH)$}$^+$ ion prevails in the present MOFs. The effect of the {$NR_3(CH_2COOH)$}$^+$ ions upon the proton conduction is explained by the net hydrophilicity tuned by the NR_3 residue.[20] The hydrophilicity of the cation affects the interlayer hydrophilicity, which is closely related to the water adsorption in the interlayer space and hence to the proton conduction. In the present case, the Et−MOFs of the more hydrophilic {$NEt_3(CH_2COOH)$}$^+$ ion are formed as dihydrate and show high proton conduction, whereas the Bu−MOFs of the less hydrophilic {$NBu_3(CH_2COOH)$}$^+$ ion are formed as anhydrate and show moderate proton conduction.

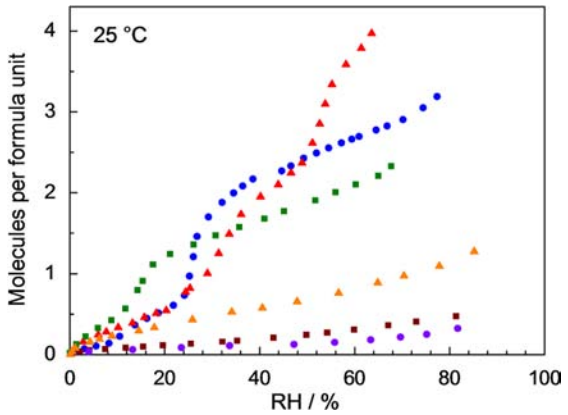

Figure 9. Water adsorption isotherms of dehydrated (blue) **Et−MnCr**, (red) **Et−FeCr**, (green) **Et−FeFe**, (purple) **Bu−MnCr**, (orange) **Bu−FeCr**, and (brown) **Bu−FeFe**.

To gain an insight into the proton conduction mechanism, the water adsorption isotherms were measured using dehydrated samples (Figure 9). The isotherm of dehydrated **Et−MnCr** shows the adsorption of two water molecules from 25% RH to 40% RH, followed by the gradual adsorption of one water molecule from 50% RH to 80% RH. Dehydrated **Et−FeCr** has a two-step isotherm with the adsorption of two water molecules at 35−50% RH followed by the adsorption of a further two water molecules at 55−65% RH. In dehydrated **Et−FeFe**, the water adsorption begins around 15% RH and reaches a near plateau of two water molecules adsorbed at 50−60% RH. The isotherms of the Et−MOFs below 50% RH are consistent with their dihydrate formulation identified in the preparation section. Under RH higher than 50% RH, the isotherms differ somewhat from each other. This may reflect the flexibility of the layered structure of the MOFs in which the layer/cation interaction can be varied by the change in the $M_a^{II}M_b^{III}$ combination.

The isotherms of the Bu-MOFs show a gradual adsorption of a small amount of water. The water molecules adsorbed at 90% RH are ~0.2 for **Bu−MnCr**, ~1.3 for **Bu−FeCr**, and ~0.4 for **Bu−FeFe**. Because there is virtually no lattice water at low RH conditions, the Bu−MOFs allow us to inspect the mechanistic function of the carboxyl residues in the proton conduction. In

dx.doi.org/10.1021/ja309968u | J. Am. Chem. Soc. 2013, 135, 2256−2262

the R−M_aM_b MOFs, the carboxyl groups at the adjacent honeycomb cavities are separated by an average O-(carboxyl)···O(carboxyl) distance of ∼7.5 Å. Thus, under low RH conditions, proton transport through hydrogen bonding (Grotthuss mechanism[47]) can be ruled out. Instead, we propose the successive hopping of a carboxyl proton to a neighboring carboxyl oxygen as the proton transport mechanism. The proton conduction in the Bu-MOFs is drastically enhanced by a slight adsorption of water. It is presumed that the adsorbed water molecules serve as mediators between the neighboring carboxyl residues through hydrogen bond formation (Grotthuss mechanism) or as the vehicles to carry protons as hydronium ions (vehicle mechanism[48]). Such cooperation of the carboxyl residues and the lattice water molecules must also occur in proton conduction in the Et−MOFs. The significance of both proton carriers and lattice water molecules in proton conduction is represented by $(NH_4)_2(adp)[Zn_2(ox)_3]\cdot 3H_2O$ (adp = adipic acid),[14] in which a high proton conductivity of 8×10^{-3} S cm^{-1} at 98% RH is induced by adipic acid as the proton carrier as well as the lattice water molecules, but the conductivity reduces to 6×10^{-6} S cm^{-1} at 70% RH because of partial dehydration to $(NH_4)_2(adp)[Zn_2(ox)_3]\cdot 2H_2O$.

From the above experimental results, the R−MnCr and R−FeCr MOFs show proton conduction and ferromagnetism, whereas the R−FeFe MOFs show proton conduction and Néel N-type ferrimagnetism. It is notable that the mixed-valence R−FeFe MOFs are the first example showing the rare Néel N-type ferrimagnetism and proton conduction. From the viewpoint of functional materials, a cooperative function of proton conduction and magnetism is of great importance. Ohkoshi has reported that the magnetic ordering in $V[Cr(CN)_6]_{2/3}\cdot nH_2O$ gives rise to a reduction in the proton conduction through a change in the crystal structure.[49] To the best of our knowledge, cooperation of proton conduction and magnetism in an exact sense has not been reported. In our attempt to examine the magnetization effect upon the proton conduction in **Et−FeFe**·$2H_2O$, it was impossible to measure the proton conductivity below 100 K because of the low conductivity (less than 10^{-12} S cm^{-1}), which decreased at lower temperatures. The interplay between proton conduction and magnetization (spin-protonics) might be inspected using MOFs with both high magnetic ordering temperature and appreciably high proton conduction. Studies in this line are under consideration.

CONCLUSIONS

MOFs of the formula $\{NR_3(CH_2COOH)\}[M_a^{II}M_b^{III}(ox)_3]$ (abbreviated as R−M_aM_b) were prepared: **Et−MnCr**·$2H_2O$, **Et−FeCr**·$2H_2O$, **Et−FeFe**·$2H_2O$, **Bu−MnCr**, **Bu−FeCr**, and **Bu−FeFe**. The crystallographic study of **Bu−MnCr** revealed oxalate-extended bimetallic layers interleaved by $\{NR_3(CH_2COOH)\}^+$ ions. The cationic ions are perpendicularly aligned to the bimetallic layers with the carboxyl residues in each honeycomb cavity. The carboxyl terminal is nearly exposed to the interlayer space so as to function as a proton carrier. **Et−MnCr**·$2H_2O$ and **Bu−MnCr** show ferromagnetic ordering with T_C of 5.6−5.9 K and **Et−FeCr**·$2H_2O$ and **Bu−FeCr** also show ferromagnetic ordering with T_C of 11.0−11.5 K. **Et−FeFe**·$2H_2O$ and **Bu−FeFe** belong to class II of mixed-valence compounds and show a Néel N-type ferrimagnetic ordering with T_C of 42−44 K. The Et−MOFs (**Et−MnCr**·$2H_2O$, **Et−FeCr**·$2H_2O$, and **Et−FeFe**·$2H_2O$) show higher proton conduction than the Bu−MOFs (**Bu−MnCr**, **Bu−FeCr**, and **Bu−FeFe**) irrespective of the magnetic nature varying with the $M_a^{II}M_b^{III}$ pair. The efficient proton conduction of the Et−MOFs relative to the Bu−MOFs is explained by the relative hydrophilicity of the cationic ions. In the Bu−MOFs having no lattice water, proton transport by a proton-hopping mechanism is recognized for the first time. The R−MnCr MOFs and the R−FeCr MOFs are a few examples of coexistent ferromagnetism and proton conduction, and the R−FeFe MOFs are the first example of coexistent Néel N-type ferrimagnetism and proton conduction.

ASSOCIATED CONTENT

Supporting Information

TGA curves of R−M_aM_b, weak-field magnetization and ac magnetization of **Bu−MnCr**, **Et−FeCr**·$2H_2O$, and **Bu−FeCr**, dM/dT vs T plots of **Et−FeFe**·$2H_2O$, χ_M vs T and μ_{eff} vs T curves and weak-field magnetization of **Bu−FeFe**. This material is available free of charge via the Internet at http://pubs.acs.org.

AUTHOR INFORMATION

Corresponding Author

*E-mail: kitagawa@kuchem.kyoto-u.ac.jp, okawa134@ac.auone-net.jp.

Present Addresses

[#]International Institute for Carbon-Neutral Energy Research (WPI-I2CNER), Kyushu University, Moto-oka 744, Nishi-ku, Fukuoka, 819−0395, Japan

[‖]Center for Molecular Systems (CMS), Department of Chemistry and Biochemistry, Graduate School of Engineering, Kyushu University, Moto-oka 744, Nishi-ku, Fukuoka, 819−0395, Japan

Notes

The authors declare no competing financial interest.

ACKNOWLEDGMENTS

This work was partly supported by the Grants-in-Aid for the Global COE Program, "Science for Future Molecular Systems" from the Ministry of Education, Culture, Science, Sports and Technology of Japan.

REFERENCES

(1) Colomban, P. *Chemistry of Solid State Chemistry 2. Proton Conductors*; Cambridge Univ. Press, 1992.

(2) Service, R. F. *Science* **2002**, *296*, 1222.

(3) Halle, S. M.; Boysen, D. A.; Chisholm, C. R. I.; Merle, R. B. *Nature* **2001**, *410*, 910.

(4) (a) Kreuer, K. D. *Chem. Mater.* **1996**, *8*, 610. (b) Kreuer, K. D. *Solid State Ionics* **1997**, *97*, 1.

(5) Marritz, K. A.; Moore, R. B. *Chem. Rev.* **2004**, *104*, 4535.

(6) Sumner, J. J.; Creager, S. E.; Ma, J. J.; DesMarTeau, D. D. *J. Electrochem. Soc.* **1998**, *145*, 107.

(7) Kreuer, K. D. *J. Membr. Sci.* **2001**, *185*, 29.

(8) Woudenberg, R. C.; Yavuzcetin, O.; Touminen, M. T.; Coughlin, E. B. *Solid State Ionics* **2007**, *178*, 1135.

(9) Li, G. H.; Lee, C. H.; Lee, Y. M.; Cho, C. G. *Solid State Ionics* **2006**, *177*, 1083.

(10) Halla, J. D.; Mamak, M.; Williams, D. E.; Ozin, G. A. *Adv. Funct. Mater.* **2003**, *13*, 133.

(11) Akutsu-Sato, A.; Akutsu, H.; Turner, S. S.; Day, P.; Probert, M. R.; Howard, J. A. K.; Akutagawa, T.; Takeda, S.; Nakamura, T.; Mori, T. *Angew. Chem.* **2005**, *117*, 296.

(12) (a) Fujishima, M.; Kanda, S.; Mitani, T.; Kitagawa, H. *Synth. Met.* **2001**, *119*, 485. (b) Nagao, Y.; Ikeda, R.; Kanda, S.; Kubozono,

Y.; Kitagawa, H. *Mol. Cryst. Liq. Cryst.* **2002**, *379*, 89. (c) Nagao, Y.; Fujishima, M.; Kanda, S.; Ikeda, R.; Kitagawa, H. *Synth. Met.* **2003**, *133*−*134*, 431. (d) Nagao, Y.; Ikeda, R.; Iijima, K.; Kubo, T.; Nakasuji, K.; Kitagawa, H. *Synth. Met.* **2003**, *135*−*136*, 283. (e) Nagao, Y.; Kubo, T.; Nakasuji, K.; Ikeda, R.; Kojima, T.; Kitagawa, H. *Synth. Met.* **2005**, *154*, 89. (f) Fujishima, M.; Enyo, M.; Kanda, S.; Ikeda, R.; Kitagawa, H. *Chem. Lett.* **2006**, *35*, 546.

(13) Yamada, T.; Sadakiyo, M.; Kitagawa, H. *J. Am. Chem. Soc.* **2009**, *131*, 3144.

(14) Sadakiyo, M.; Yamada, T.; Kitagawa, H. *J. Am. Chem. Soc.* **2009**, *131*, 9906.

(15) (a) Morikawa, S.; Yamada, T.; Kitagawa, H. *Chem. Lett.* **2009**, 654. (b) Yamada, T.; Morikawa, S.; Kitagawa, H. *Bull. Chem. Soc. Jpn.* **2010**, *83*, 42.

(16) Bureekaew, S.; Horike, S.; Higuchi, M.; Mizuno, M.; Kawamura, T.; Tanaka, D.; Yanai, N.; Kitagawa, S. *Nat. Mater.* **2009**, *8*, 831.

(17) Kanaizuka, K.; Iwakiri, S.; Yamada, T.; Kitagawa, H. *Chem. Lett.* **2010**, 28.

(18) (a) Hurd, J. A.; Vaidhyanathan, R.; Thangadurai, V.; Ratcliffe, C. I.; Moudrakovski, I. L.; Shimizu, G. K. H. *Nat. Chem.* **2009**, *1*, 705. (b) Taylor, J. M.; Mah, R. K.; Moudrakovski, I. L.; Ratcliffe, C. I.; Valdhyanathan, R.; Shimizu, G. K. H. *J. Am. Chem. Soc.* **2010**, *132*, 14055.

(19) Ōkawa, H.; Sadakiyo, M.; Shigematsu, A.; Miyakawa, T.; Ohba, M.; Kitagawa, H. *J. Am. Chem. Soc.* **2009**, *131*, 13516.

(20) Sadakiyo, M.; Ōkawa, H.; Shigematsu, A.; Ohba, M.; Yamada, T.; Kitagawa, H. *J. Am. Chem. Soc.* **2012**, *134*, 5472.

(21) (a) Zhong, Z. J.; Matsumoto, N.; Ōkawa, H.; Kida, S. *Chem. Lett.* **1990**, 87. (b) Tamaki, H.; Zhong, Z. J.; Matsumoto, N.; Kida, S.; Koikawa, M.; Achiwa, N.; Hashimoto, Y.; Ōkawa, H. *J. Am. Chem. Soc.* **1992**, *114*, 6974.

(22) (a) Decurtins, S.; Schmalle, H. W.; Oswald, H. R.; Linden, A.; Ensling, J.; Gütlich, P.; Hauser, A. *Inorg. Chim. Acta* **1994**, *216*, 65. (b) Pellaux, R.; Schmalle, H. W.; Huber, R.; Fisher, P.; Hauss, T.; Ouladdiaf, B.; Decurtins, S. *Inorg. Chem.* **1997**, *36*, 2301.

(23) Coronado, E.; Galán-Mascarós, J. R.; Gómez-García, C. J.; Ensling, J.; Gütlich, P. *Chem.—Eur. J.* **2000**, *6*, 552.

(24) (a) Bénard, S.; Rivière, E.; Yu, P.; Nakatani, K.; Delouis, J. F. *Chem. Mater.* **2001**, *13*, 159. (b) Bénard, S.; Yu, P.; Audière, J. P.; Rivière, E.; Clément, R.; Guilhem, J.; Tchertanov, L.; Nakatani, K. *J. Am. Chem. Soc.* **2000**, *122*, 9444.

(25) (a) Coronado, E.; Galán-Mascarós, J. R.; Gómez-Garcia, C. J.; Laukhln, V. *Nature* **2000**, *408*, 447. (b) Alberola, A.; Coronado, E.; Galán-Mascarós, J. R.; Giménez-Saiz, C.; Gómez-García, C. J.; Romero, F. M. *Synth. Met.* **2003**, *133*−*134*, 509. (c) Alberola, A.; Coronado, E.; Galán-Mascarós, J. R.; Giménez-Saiz, C.; Gómez-García, C. J.; Martínez-Ferrero, E.; Murcia-Martínez, A. *Synth. Met.* **2003**, *135*−*136*, 687. (d) Alberola, A.; Coronado, E.; Galán-Mascarós, J. R.; Giménez-Saiz, C.; Gómez-García, C. J. *J. Am. Chem. Soc.* **2003**, *125*, 10774.

(26) Train, C.; Gheorghe, R.; Krstic, V.; Chamoreau, L. M.; Ovanesyan, N. S.; Rikken, G. L. J. A.; Gruselle, M.; Verdaguer, M. *Nat. Mater.* **2008**, *7*, 729.

(27) Bailar, J. C., Jr.; Jones, E. M. *Inorg. Synth.* **1939**, *1*, 36.

(28) Landolt-Börnstein, Neue Series II/11; Springer-Verlag, Berlin (1981).

(29) Opekar, F.; Svozil, D. *J. Electroanal. Chem.* **1995**, *385*, 269.

(30) CrystalStructure 3.8.0: Crystal Structure Analysis Package, Rigaku and Rigaku/MSC (2000 − 2006).

(31) SHELX97: Sheldrick, G. M. (1997).

(32) (a) Miyazato, Y.; Ohba, M.; Sakiyama, H.; Ōkawa, H. *Bull. Chem. Soc. Jpn.* **2007**, *80*, 1534. (b) Miyazato, Y.; Ohba, M.; Hayami, S.; Maeda, Y.; Tadokoro, M.; Ōkawa, H. *Chem. Lett.* **2009**, *38*, 24.

(33) Suzuki, M.; Uehara, A. *Inorg. Chim. Acta* **1986**, *123*, L9.

(34) (a) Borovik, A. S.; Murch, B. P.; Que, L., Jr.; Papaefthymiou, V.; Münck, H. *J. Am. Chem. Soc.* **1987**, *109*, 7190. (b) Borovik, A. S.; Que, L., Jr. *J. Am. Chem. Soc.* **1988**, *110*, 2345.

(35) Dutta, S. K.; Ensling, J.; Werner, R.; Flörke, U.; Haase, W.; Gütlich, P.; Nag, K. *Angew. Chem., Int. Ed. Engl.* **1977**, *36*, 152.

(36) Mashuta, M. S.; Webb, R. J.; McCusker, J. K.; Schmitt, E. A.; Oberhausen, K. J.; Richardson, J. F.; Buchanan, R. M.; Hendrickson, D. N. *J. Am. Chem. Soc.* **1992**, *114*, 3815.

(37) Robin, M. B.; Day, P. *Advan. Inorg. Chem. Radiochem.* **1967**, *10*, 247.

(38) (a) Tamaki, H.; Mitsumi, M.; Nakamura, K.; Matsumuto, N.; Kida, S.; Ōkawa, H.; Iijima, S. *Chem. Lett.* **1992**, 1975. (b) Ōkawa, H.; Matsumoto, N.; Tamaki, H.; Ohba, M. *Mol. Cryst. Liq. Cryst.* **1993**, *233*, 257.

(39) (a) Mathoniere, C.; Carling, S. G.; Yusheng, D.; Day, P. *J. Chem. Soc., Chem. Commun.* **1994**, 1551. (b) Mathoniere, C.; Nuttall, C. J.; Carling, S. G.; Day, P. *Inorg. Chem.* **1996**, *35*, 1201. (c) Nuttall, C. J.; Day, P. *Chem. Mater.* **1998**, *10*, 3050. (d) Carling, S. G.; Day, P.; Nuttall, C. *J. Spectrochimica Acta Part A* **2001**, *57*, 1971. (e) Watts, I. D.; Carling, S. G.; Day, P. *Phys. Chem. Chem. Phys.* **2001**, *3*, 4418. (f) Watts, I. D.; Carling, S. G.; Day, P. *J. Chem. Soc., Dalton. Trans.* **2002**, 1429.

(40) Néel, L. *Ann. Phys.* **1948**, *3*, 137.

(41) Tung, L. D.; Lees, M. R.; Balakrishnan, G.; Paul, D. M. *Phys. Rev. B* **2007**, *75*, 104404.

(42) Kimishima, Y.; Ichiyanagi, Y.; Shimizu, K.; Mizuno, J. *Magn. Magn. Mater.* **2000**, *210*, 244.

(43) Yoshii, K.; Nakamura, A.; Ishii, Y.; Morii, Y. J. *Solid State Chem.* **2001**, *162*, 84.

(44) Cooke, A. H.; Martin, D. M.; Wells, M. R. *J. Phys. C: Solid State Phys.* **1974**, *7*, 31333.

(45) Hagen, K. S.; Naik, S. G.; Huynh, B. H.; Masello, A.; Christou, G. *J. Am. Chem. Soc.* **2009**, *131*, 7516.

(46) Zhao, J.; Hu, B.; Lloret, F.; Tao, J.; Yang, Q.; Zhang, X.; Bu, X. *Inorg. Chem.* **2010**, *49*, 10390.

(47) (a) Howe, A. T.; Shilton, M. G. *J. Solid State Chem.* **1980**, *24*, 149. (b) Bernard, L.; Fitch, A.; Wright, A. F.; Fender, B. E. F.; Howe, A. T. *Solid State Ionics* **1981**, *5*, 459.

(48) Kreuer, K. D.; Rabenau, A.; Weppner, W. *Angew. Chem., Int. Ed.* **2004**, *21*, 208.

(49) Ohkoshi, S.; Nakagawa, K.; Tomono, K.; Imoto, K.; Tsunobuchi, Y.; Tokoro, H. *J. Am. Chem. Soc.* **2010**, *132*, 6620.